

SN 2012AU: A GOLDEN LINK BETWEEN SUPERLUMINOUS SUPERNOVAE AND THEIR LOWER-LUMINOSITY COUNTERPARTS

DAN MILISAVLJEVIC¹, ALICIA M. SODERBERG¹, RAFFAELLA MARGUTTI¹, MARIA R. DROUT¹, G. HOWIE MARION¹,
NATHAN E. SANDERS¹, ERIC Y. HSIAO², RAGNHILD LUNNAN¹, RYAN CHORNOCK¹, ROBERT A. FESEN³,
JEROD T. PARRENT^{3,4}, EMILY M. LEVESQUE⁵, EDO BERGER¹, RYAN J. FOLEY¹, PETE CHALLIS¹, ROBERT P. KIRSHNER¹,
JASON DITTMANN¹, ALLYSON BIERYLA¹, ATISH KAMBLE¹, SAYAN CHAKRABORTI¹, GISELLA DE ROSA⁶,
MICHAEL FAUSNAUGH⁶, KEVIN N. HAINLINE³, CHIEN-TING CHEN³, RYAN C. HICKOX³, NIDIA MORRELL²,
MARK M. PHILLIPS², MAXIMILIAN STRITZINGER⁷

Accepted to ApJL on May 2, 2013

ABSTRACT

We present optical and near-infrared observations of SN 2012au, a slow-evolving supernova (SN) with properties that suggest a link between subsets of energetic and H-poor SNe and superluminous SNe. SN 2012au exhibited conspicuous SN Ib-like He I lines and other absorption features at velocities reaching $\approx 2 \times 10^4$ km s⁻¹ in its early spectra, and a broad light curve that peaked at $M_B = -18.1$ mag. Models of these data indicate a large explosion kinetic energy of $\sim 10^{52}$ erg and ⁵⁶Ni mass ejection of $M_{\text{Ni}} \approx 0.3M_{\odot}$ on par with SN 1998bw. SN 2012au's spectra almost one year after explosion show a blend of persistent Fe II P-Cyg absorptions and nebular emissions originating from two distinct velocity regions. These late-time emissions include strong [Fe II], [Ca II], [O I], Mg I, and Na I lines at velocities $\gtrsim 4500$ km s⁻¹, as well as O I and Mg I lines at noticeably smaller velocities $\lesssim 2000$ km s⁻¹. Many of the late-time properties of SN 2012au are similar to the slow-evolving hypernovae SN 1997dq and SN 1997ef, and the superluminous SN 2007bi. Our observations suggest that a single explosion mechanism may unify all of these events that span $-21 \lesssim M_B \lesssim -17$ mag. The aspherical and possibly jetted explosion was most likely initiated by the core collapse of a massive progenitor star and created substantial high-density, low-velocity Ni-rich material.

Subject headings: supernovae: general — supernova: individual (SN 2012au)

1. INTRODUCTION

Recent transient surveys (e.g., the Panoramic Survey Telescope and Rapid Response System, the Palomar Transient Factory, the Catalina Real-Time Transient Survey [CRTS], the Texas Supernova Search now operating as the ROTSE Supernova Verification Project) and growing support from amateur observers have uncovered ever-increasing diversity in the observational properties of supernovae (SNe). Indeed, the standard classification system Type I and Type II originally proposed by Minkowski (1941) has branched considerably from its binary roots, and is continually being updated in the face of new objects that bridge subtypes and extend luminosity ranges.

Some of the more luminous H- and He-poor SNe discovered by these efforts have garnered especial attention because of their connection with long-duration gamma-ray bursts (GRBs; see Hjorth & Bloom 2012 for a recent

review). Strong evidence for this relationship came from multi-wavelength observations of SN 1998bw, a broad-lined SN Ic coincident with GRB980425, and belonging to an energetic class of explosions reaching $\sim 10^{52}$ erg called hypernovae (Galama et al. 1998; Iwamoto et al. 1998). The handful of energetic broad-lined SN Ic that have been well-observed vary considerably in their properties and are not always accompanied with GRBs, e.g., SN 1997ef (Iwamoto et al. 2000).

superluminous SNe (SLSNe) with absolute magnitudes of $\lesssim -21$ are recent members of the growing SN classification zoo (Quimby et al. 2011). H-poor examples can be even more powerful than SNe Ic (Gal-Yam 2012), and there has been considerable effort to understand their nature and relationship with more typical SNe. One of the first examples of the H-poor variety was SN 2007bi (Gal-Yam et al. 2009; Young et al. 2010), which was originally suggested to be the result of the pair-instability explosion mechanism (Barkat et al. 1967). Alternative interpretations, however, have been offered (Dessart et al. 2012, 2013), including those involving a central engine magnetar (Kasen & Bildsten 2010), interaction with circumstellar shells (Chatzopoulos & Wheeler 2012), or Fe core collapse (Moriya et al. 2010; Yoshida & Umeda 2011). To date, no SLSN has been observationally connected to a GRB.

Here we report photometric and spectroscopic data on SN 2012au, an object that suggests a link between some subtypes of energetic and H-poor SNe and SLSNe. Although initial spectroscopic observations showed prominent helium absorption features of an otherwise ordinary

¹ Harvard-Smithsonian Center for Astrophysics, 60 Garden Street, Cambridge, MA, 02138.

Electronic address: dmilisav@cfa.harvard.edu

² Carnegie Observatories, Las Campanas Observatory, Colina El Pino, Casilla 601, Chile

³ 6127 Wilder Lab, Department of Physics & Astronomy, Dartmouth College, Hanover, NH, 03755

⁴ Las Cumbres Observatory Global Telescope Network, Goleta, CA, US

⁵ CASA, Department of Astrophysical and Planetary Sciences, University of Colorado, 389-UCB, Boulder, CO 80309, USA

⁶ Department of Astronomy, The Ohio State University, 140 West 18th Avenue, Columbus, OH 43210, USA

⁷ Department of Physics and Astronomy, Aarhus University, Ny Munkegade 120, DK-8000 Aarhus C, Denmark

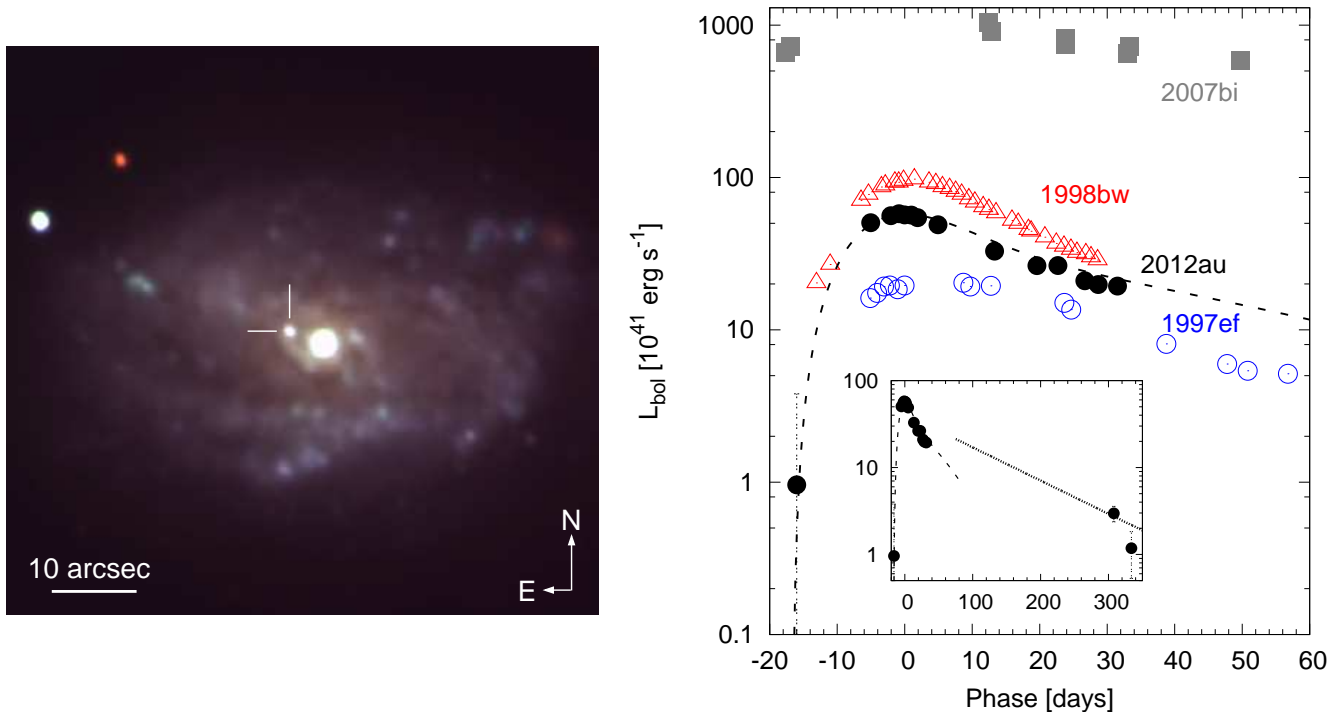


Figure 1. Left: Image of the region around SN 2012au (marked) and its host galaxy NGC 4790 made from MMTcam $g'r'i'$ images obtained 2013 February 18. Right: Reconstructed pseudo-bolometric light curve of SN 2012au and our radioactive decay diffusion model fit for photospheric (dashed line) and nebular (dotted line, inset) epochs. Phase is in the rest-frame and with respect to maximum light. Also shown are bolometric light curves of SN 1997ef (Nomoto et al. 2000), SN 1998bw (Maeda et al. 2006), and SN 2007bi (Gal-Yam 2012).

SN Ib (Silverman et al. 2012; Soderberg et al. 2012), continued monitoring of SN 2012au through to nebular stages ($t > 250$ d) revealed extraordinary emission properties in its optical and near-infrared spectra that prompted this *Letter*. A complementary analysis of SN 2012au’s radio and X-ray emissions is forthcoming in Kamble et al. (in prep).

2. OBSERVATIONS AND RESULTS

2.1. UV and Optical Photometry

SN 2012au was discovered on 2012 March 14 UT by the CRTS SNHunt project (Howerton et al. 2012). Figure 1 (left) shows the region around the SN and its host galaxy NGC 4790 ($D = 23.5 \pm 0.5$ Mpc; Theureau et al. 2007). SN 2012au is located at coordinates $\alpha = 12^{\text{h}}54^{\text{m}}52^{\text{s}}.18$ and $\delta = -10^{\circ}14'50''.2$ (J2000.0), which is less than 600 pc away in projection from the center of NGC 4790’s bright central nucleus.

Ultra-violet (UV) and optical observations with the *Swift*-UVOT instrument began 2012 March 15 and continued through to 2012 April 21 (PI P. Brown). Data were acquired using six broad band filters and have been analyzed following standard procedures. The details of these *Swift*-UVOT observations are provided in Table 1.

Two epochs of late-time r' -band photometry of SN 2012au were obtained. A sequence of 3×300 s dithered images were taken on 2013 January 23 using the 2.4m Hiltner telescope at MDM Observatory with the OSMOS instrument⁸ and MDM4k detector, and a sequence of 3×120 s dithered images were taken on 2013 Feb 18 using the 6.5m MMT with the MMTcam instru-

ment⁹. Images were bias-subtracted, flat-fielded, and stacked following standard procedures using the IRAF¹⁰ software.

Emission from SN 2012au dropped $\lesssim 4$ mag between maximum light and our first late-time measurement 308 days later. This decline is considerably slower than other SNe Ib/c; e.g., SN 1998bw declined by ≈ 6.5 mag over the same time period (Patat et al. 2001). The longevity of the brightness made it impossible to obtain subtraction templates that could completely remove contaminating emission from the underlying host galaxy. Photometric measurements were thus made using the *sextractor* software (Bertin & Arnouts 1996) and checked manually using point-spread-function fitting techniques.

2.2. A Model of the Bolometric Light Curve

We constructed a pseudo-bolometric light curve using the *Swift*-UVOT photometry. Observations were corrected assuming $R_V = A_V/E(B-V) = 3.1$ and a total reddening of $E(B-V) = 0.063$ mag. This estimate combines reddening due to the Milky Way, $E(B-V)_{mw} = 0.043$ mag (Schlafly & Finkbeiner 2011), and host internal extinction of $E(B-V)_{host} = 0.02 \pm 0.01$ mag determined from measuring the equivalent width (EW) of Na I D absorption in our optical spectra (Section 2.3) and using the relationship between EW and $E(B-V)$ described in Poznanski et al. (2012).

The pseudo-bolometric light curve incorporates two

⁹ <http://www.cfa.harvard.edu/mmti/wfs.html>

¹⁰ IRAF is distributed by the National Optical Astronomy Observatory, which is operated by the Association of Universities for Research in Astronomy (AURA) under cooperative agreement with the National Science Foundation.

⁸ <http://www.astronomy.ohio-state.edu/~martini/osmos/>

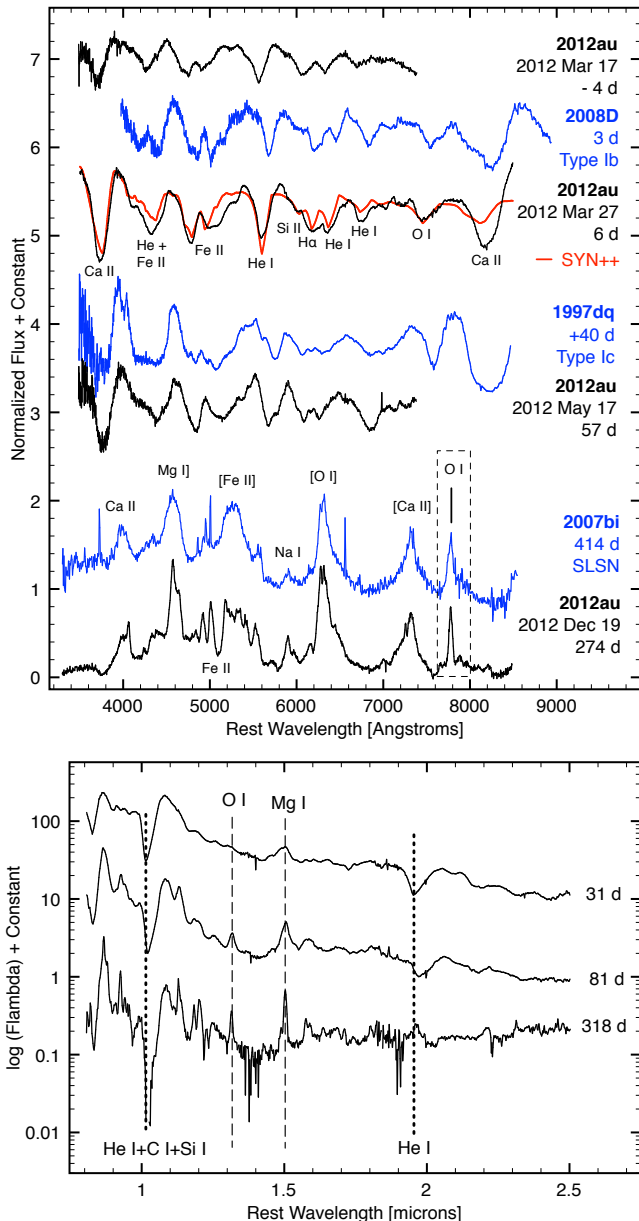


Figure 2. Top: Optical spectra of SN 2012au. In red is the SYN++ synthetic spectrum. Also shown are SN 2008D (Soderberg et al. 2008), SN 1997dq (Matheson et al. 2001), and SN 2007bi (Gal-Yam et al. 2009). Spectra have been normalized according to the procedure outlined in Jeffery et al. (2007). Bottom: Near-infrared spectra of SN 2012au. The heavy dotted lines highlight He I absorptions, and the light dashed lines highlight O I and Mg I emission features.

values from Howerton et al. (2012), one of which is a detection of the SN on 2012 March 4 that constrains the rise time from explosion to peak brightness to be $\gtrsim 16$ days. We summed the flux emitted in the *uvw2* through *v* bands by means of a trapezoidal interpolation and estimated the missing flux from the *RI* passbands and the near-infrared around the time of maximum light, t_{\max} . Using values observed in other SNe Ib/c (see Valenti et al. 2008), we assumed that for $-5 < \Delta t_{\max} < 30$ d, the *RI*-band flux contribution varies from 25% to 40% and the near-infrared band contribution varies from 15% to 45%.

The pseudo-bolometric light curve was modeled using assumptions in Arnett (1982) and following procedures in Valenti et al. (2008) to determine the SN’s total nickel mass, M_{Ni} , explosion kinetic energy, E_{K} , and total ejecta mass M_{ej} . A constant optical opacity k_{opt} of $0.05 \text{ cm}^2 \text{ g}^{-1}$ was adopted (see Drout et al. 2011 for details). Our best-fit model shown in Figure 1 (right) uses the explosion date 2012 March 3.5, and a rise time of 16.5 ± 1.0 d. The peak bolometric luminosity is $\sim 6 \times 10^{42} \text{ erg s}^{-1}$, and the estimates of the explosion parameters are $M_{\text{Ni}} \approx 0.3 M_{\odot}$, $M_{\text{ej}} \approx 3 - 5 M_{\odot}$, and $E_{\text{K}} \sim 1 \times 10^{52} \text{ erg}$.

We break the degeneracy between E_{K} and M_{ej} using an estimate of the ejecta velocity measured from our optical spectra around t_{\max} to be $\approx 1.5 \times 10^4 \text{ km s}^{-1}$ (Section 2.3). The value of M_{Ni} is consistent with independent estimates derived from the late-time photometry under the assumption of full gamma-ray trapping (Figure 1, right, inset). These explosion parameters are comparable to those estimated for the hypernovae SN 1998bw ($M_{\text{Ni}} \sim 0.4 M_{\odot}$ and $E_{\text{K}} \sim 2 \times 10^{52} \text{ erg}$; Maeda et al. 2006) and SN 1997ef ($M_{\text{Ni}} \sim 0.16 M_{\odot}$ and $E_{\text{K}} \sim 1 \times 10^{52} \text{ erg}$; Iwamoto et al. 2000).

We note that SN 2012au may exhibit properties that are not strictly incorporated in the Arnett (1982) model we have used. Opacities as high as $0.2 \text{ cm}^2 \text{ g}^{-1}$ could apply that increase the $M_{\text{Ni}}/M_{\text{ej}}$ ratio to values that run contrary to model assumptions, and optical spectra (Section 2.4) suggest possible deviations from the model’s spherically symmetric conditions. Future work may look to apply more sophisticated models to address these additional factors.

2.3. Optical Spectroscopy ($t < 60$ day)

Low-resolution optical spectra of SN 2012au were obtained from March 2012 through Feb 2013. Many of these observations were made with the F. L. Whipple Observatory 1.5-m telescope mounted with the FAST instrument (Fabricant et al. 1998). Additional observations were obtained with the MMT 6.5m telescope using the Blue Channel instrument (Schmidt et al. 1989), and the 2.4m MDM telescope using the OSMOS instrument.

Standard procedures using the IRAF software were followed and flux calibrations were made using our own IDL routines. A recession velocity of 1295 km s^{-1} determined from overlapping nebular $\text{H}\alpha$ emission has been removed from all spectra. Line identifications and estimates of expansion velocities of the photospheric spectra were made with the supernova spectrum synthesis code SYN++ (Thomas et al. 2011).

Four epochs of our optical spectra of SN 2012au are plotted in Figure 2 (top). The reported phase is with respect to *v*-band maximum on 2012 March 21. Our earliest spectrum obtained 2012 Mar 17 ($\Delta t_{\max} = -4$ d) shows features associated with He I, Fe II, Si II, Ca II, Na I, and O I exhibiting velocities of $(1.8 - 2.0) \times 10^4 \text{ km s}^{-1}$. There is weak evidence of $\text{H}\alpha$ absorption.

We show a slightly later spectrum obtained 2012 Mar 27 ($\Delta t_{\max} = +6$ d) in Figure 2 (top) illustrating how the identified ions are generally consistent with a Type Ib classification (e.g., SN 2008D) though the velocities in SN 2012au are relatively high. Approximately two months later on 2012 Mar 17 ($\Delta t_{\max} = +57$ d), the same ions are detected but the Type Ib classification

is less appropriate. The observed velocities (~ 7000 km s $^{-1}$) remain above average relative to other SNe Ib/c at this epoch, the P-Cyg absorptions broaden, and the spectrum resembles those of SN 1997dq and SN 1997ef (Matheson et al. 2001).

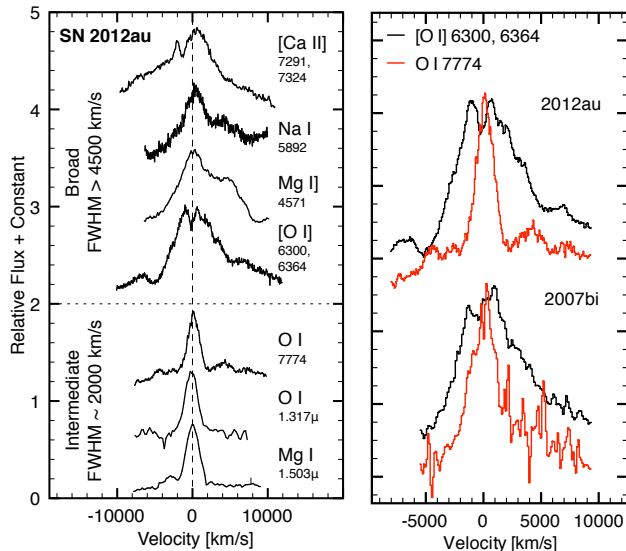


Figure 3. Left: Late-time emission line profiles of SN 2012au. Profiles are grouped by broad ($\text{FWHM} \gtrsim 4500$ km s $^{-1}$) and intermediate ($\text{FWHM} \sim 2000$ km s $^{-1}$) widths. Right: The O I $\lambda 7774$ and [O I] $\lambda\lambda 6300, 6364$ emission line profiles of SN 2012au and SN 2007bi.

2.4. Optical Spectroscopy ($t > 250$ day)

The defining properties of SN 2012au are seen in its nebular spectrum (Figure 2, top). Emissions from SNe Ib/c at these epochs are normally optically thin and dominated by [O I] $\lambda\lambda 6300, 6364$, [Ca II] $\lambda\lambda 7291, 7324$, and Mg I] $\lambda 4571$. In addition to these emissions, however, SN 2012au shows persistent P-Cyg absorptions attributable in part to Fe II at $\lesssim 2000$ km s $^{-1}$, as well as unusually strong emissions from Ca II H&K, Na I D, and a feature around 7775 Å we identify as O I $\lambda 7774$.

Also seen in the nebular spectrum is a “plateau” of emission between $4000 - 5600$ Å. This emission is due largely to iron-peak elements (primarily [Fe II], and some [Fe III] and [Co II]), which is usually only observed with this strength in the late-time spectra of SNe Ia. Unlike SNe Ia, however, here the [Fe III] lines are weak.

In Figure 3 (left), emission line profiles of SN 2012au’s most prominent late-time spectral features are shown. There are real differences among the emission line profiles across elements and their ions. Specific features of note include: (1) the [Ca II], Na I, and Mg I] lines are not symmetric about zero velocity and exhibit higher expansion velocities than [O I], and (2) the O I and [O I] lines indicate two distinct velocity regions in the ejecta.

The relative strengths of narrow lines from coincident host galaxy emission in the nebular spectra were measured to estimate the explosion site metallicity using the method described in Sanders et al. (2012). From the N2 diagnostic of Pettini & Pagel (2004), we measure an oxygen abundance of $\log(\text{O}/\text{H}) + 12 = 8.9$ with uncertainty 0.2 dex. Adopting a solar metallicity of

$\log(\text{O}/\text{H})_{\odot} + 12 = 8.7$ (Asplund et al. 2005), the measurement indicates that SN 2012au exploded in an environment of super-solar metallicity around $Z \sim 1 - 2 Z_{\odot}$. This metallicity is significantly higher than any of the broad-lined SN Ic host galaxies from untargeted surveys (Sanders et al. 2012).

2.5. Near-Infrared Spectroscopy

Three epochs of low-resolution, near-infrared spectra spanning 0.82 to 2.51 μm were obtained using the Folded-Port Infrared Echellette (FIRE) spectrograph on the 6.5-m Magellan Baade Telescope (Simcoe et al. 2008). The low dispersion prism used in combination with a $0''.6$ slit yielded a spectral resolution $R \sim 500$ in J -band. Data were reduced following standard procedures (see, e.g., Hsiao et al. 2013) using a custom-developed IDL pipeline (FIREHOSE).

The reduced near-infrared spectra are plotted in Figure 2 (bottom). In our $\Delta t_{\text{max}} = +31$ d spectrum, absorptions around both the He I $\lambda 1.083 \mu\text{m}$ and $\lambda 2.05 \mu\text{m}$ lines support the identification of He I made in the optical spectra. The minima of these absorptions shift toward longer wavelengths in the later epochs, and the absorption around $1 \mu\text{m}$ grows in strength as the $2 \mu\text{m}$ absorption fades. This suggests that the He I strength diminishes as other ions possibly including Si I and C I gradually dominate the $1 \mu\text{m}$ absorption as time passes.

Between $\Delta t_{\text{max}} = +81$ and $+318$ d, the full-width-at-half-maximum (FWHM) of strong emission features associated with the Mg I $\lambda 1.503 \mu\text{m}$ and O I $\lambda 1.317 \mu\text{m}$ lines narrow from approximately 5700 km s $^{-1}$ to 2000 km s $^{-1}$. The presence of these lines and the similarity of their velocity distribution to the feature around 7775 Å support our identification of it being associated with O I $\lambda 7774$ (Figure 3, left).

3. DISCUSSION

3.1. Extraordinary Late-Time Emission Properties

Our UV/optical and near-infrared observations of SN 2012au show it to be a slow-evolving energetic supernova with a number of rarely observed late-time emission properties. SN 2012au’s plateau of iron emission lines, intermediate-width O I $\lambda 7774$ emission, persistent P-Cyg absorption features, and prolonged brightness almost one year after explosion are not observed in the majority of late-time spectra of SNe Ib/c (Figure 4, top).

However, a handful of objects including SN 1997dq and 2007bi do share SN 2012au’s rare blend of late-time properties. Aside from some difference in the strength and velocity widths of the Fe and Mg emissions below ≈ 5600 Å, above ≈ 5600 Å emissions from these SNe are almost indistinguishable (Figure 4, bottom). Like SN 2012au, these objects exhibited slow spectroscopic evolution and slowly declining light curves (see Mazzali et al. 2004, Gal-Yam et al. 2009, and Young et al. 2010).

Mazzali et al. (2004) interpreted the long duration of the photospheric phase in SN 1997dq and SN 1997ef to be the consequence of a sharply defined two-component ejecta distribution made of an inner, high-density region, located inside a much lower-density region of high-velocity ejecta. This was a scenario that had been previously modeled by Maeda et al. (2003). Mazzali et al. concluded that a significant fraction of Ni-rich material was

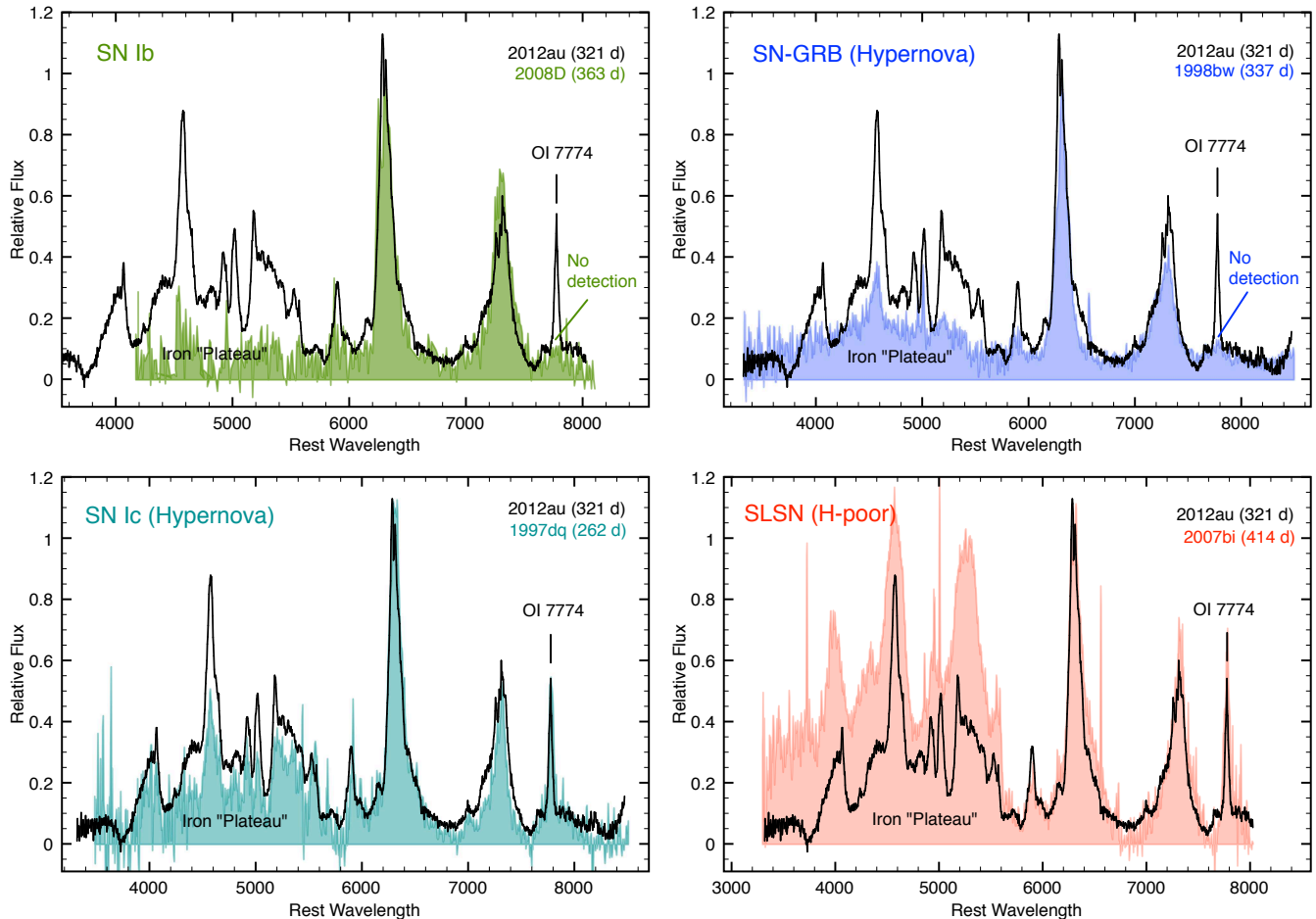


Figure 4. Late-time spectrum of SN 2012au obtained 2013 February 5 compared to those of other SNe Ib/c. Relative flux has been arbitrarily scaled to match the strength of [O I] $\lambda\lambda 6300, 6364$ emission. Top panels show the SN Ib SN 2008D (Tanaka et al. 2009) and the hypernova SN 1998bw (Patat et al. 2001), where spectroscopic evolution is normal and O I $\lambda 7774$ is not detected. These SNe are representative of late-time emissions from the majority of SNe Ib/c (see, e.g., Matheson et al. 2001; Taubenberger et al. 2009; Milisavljevic et al. 2010). Bottom panels show the hypernova SN 1997dq (Matheson et al. 2001) and the SLSN SN 2007bi (Gal-Yam et al. 2009), where spectroscopic evolution is slow, strong O I $\lambda 7774$ emission is detected, and emission from Fe lines forms an emission plateau between 4000 – 5600 Å.

associated with velocities below the normal mass cut-off imposed in one-dimensional explosion models and that this signaled the presence of explosion asymmetries.

A similar explanation may be applicable to SN 2012au. The persistent P-Cyg absorptions and asymmetries between elements and their ions in the emission line profiles are consistent with expectations of a moderately aspherical explosion. Moreover, the absence of [Fe III] in the iron plateau region (Figure 4) indicates that the density of the Fe-rich region is high and likely clumped. Thus, it is possible this asphericity was jet-driven, since models have demonstrated that jetted explosions can significantly alter density profiles and ^{56}Ni distributions, especially in the central region (Maeda & Nomoto 2003).

The presence of the density-sensitive line O I $\lambda 7774$ and its velocity width is especially noteworthy. In the cases of SN 2012au and SN 2007bi, the center of the O I distribution sits in the middle of an emission gap of the [O I] $\lambda\lambda 6300, 6364$ profile (Figure 3, right). This, along with the Mg I $1.503\mu\text{m}$ feature in the near-infrared, is suggestive of an O- and Mg-rich region with densities that are collisionally quenching some of the [O I] $\lambda\lambda 6300, 6364$ emission.

3.2. A Unified Explosion Mechanism?

On the one hand, it seems unlikely that SNe with very different peak luminosities and light curves can share progenitor systems and explosion mechanisms (Figure 1, right). SN 2007bi was a superluminous ($M_B \approx -21$ mag) explosion that ejected some $\sim 3 - 5M_\odot$ of radioactive ^{56}Ni , and was associated with a $200 M_\odot$ progenitor (ZAMS) located in a low metallicity dwarf galaxy (Gal-Yam et al. 2009; Young et al. 2010). These properties are very different from SN 2012au, which was far less luminous ($M_B \approx -18$ mag), produced an order of magnitude less ^{56}Ni , and was located in a nearby flocculent spiral we estimate to have super-solar metallicity. Moreover, we find that a comparison of Geneva stellar evolution models (Ekström et al. 2012) to results from a preliminary analysis of pre-explosion *Hubble Space Telescope* images of the region encompassing SN 2012au (Van Dyk et al. 2012) places loose limits on the progenitor star as likely being $< 80 M_\odot$.

Despite these differences, however, the combination of observed optical properties shared between these SNe is still suggestive of a unified explosion mechanism. If a connection between these objects exists, then one of the three currently favored energy mechanisms of

SLSNe powering their slow light curves should extend to SN2012au. One late-time mechanism is interaction with circumstellar material. Although no narrow emission lines ($\text{FWHM} \lesssim 100 \text{ km s}^{-1}$) have been detected, interaction with H-poor circumstellar shells from pulsational pair-instability SNe could potentially be applicable (Chatzopoulos & Wheeler 2012). Favoring against this, however, is that SN2012au's radio light curves and SED evolution are most consistent with blast wave interaction with a steady, homogeneous wind (Kamble et al., in prep). Another mechanism is injection of energy from a magnetar, but the presence of strong iron emission, as observed in SN2012au, could be problematic for this scenario (Kasen & Bildsten 2010).

A straightforward understanding of SN2012au's light curve is radioactive ^{56}Ni . The rise and fall of the light curve at photospheric epochs, and the subsequent slow decline of the light curve at the rate of $\approx 0.01 \text{ mag d}^{-1}$ up until $\sim 300 \text{ d}$, reasonably follow predictions of Ni-Co decay (Figure 1). Possible origins for the above average ^{56}Ni production may be either a pair instability explosion or Fe core collapse of a massive progenitor. A pair-instability explosion is unlikely given that the progenitor mass and metallicity we estimate for SN2012au are outside theoretical limits (see Langer et al. 2007). Hence, Fe core collapse is the prime candidate. SN2012au's exceptionally high energies suggest that the explosion may have been aided by magnetohydrodynamic jets brought about by rapid rotation (Burrows et al. 2007).

4. CONCLUSIONS

We have shown that SN2012au is an energetic ($E_K \sim 10^{52} \text{ erg}$) explosion having a rarely observed combination of late-time properties that suggest a link between subsets of energetic and H-poor SNe and SLSNe. These events, which extend over a large range of absolute magnitudes ($-21 \lesssim M_B \lesssim -17 \text{ mag}$), appear to be observationally connected by a slow spectroscopic evolution expressed by persistent P-Cyg absorptions, intermediate-width ($\sim 2000 \text{ km s}^{-1}$) O I $\lambda 7774$ emission approximately a year after explosion, and slowly declining light curves. We conclude that they may be unified in a single framework involving the core collapse of a massive progenitor and a subsequent asymmetric explosion.

We thank an anonymous for informed suggestions that improved the manuscript, and the Harvard College Observatory for supporting the Astronomy100 class who were first to classify SN2012au. Support was provided by the David and Lucile Packard Foundation Fellowship for Science and Engineering awarded to A.M.S. Additional support is from the NSF under grants AST-0306969, AST-0607438, AST-1008343, and AST-121196. Observations reported here were obtained at the MMT Observatory, a joint facility of the Smithsonian Institution and the University of Arizona, as well as the 6.5 m Magellan Telescopes located at Las Campanas Observatory, Chile. This paper used the Weizmann interactive supernova data repository (<http://www.weizmann.ac.il/astrophysics/wiserep>).

REFERENCES

- Arnett, W. D. 1982, *ApJ*, 253, 785
 Asplund, M., Grevesse, N., & Sauval, A. J. 2005, in *Astronomical Society of the Pacific Conference Series*, Vol. 336, *Cosmic Abundances as Records of Stellar Evolution and Nucleosynthesis*, ed. T. G. Barnes III & F. N. Bash, 25
 Barkat, Z., Rakavy, G., & Sack, N. 1967, *Physical Review Letters*, 18, 379
 Bertin, E., & Arnouts, S. 1996, *A&AS*, 117, 393
 Burrows, A., Dessart, L., Livne, E., Ott, C. D., & Murphy, J. 2007, *ApJ*, 664, 416
 Chatzopoulos, E., & Wheeler, J. C. 2012, *ApJ*, 760, 154
 Dessart, L., Hillier, D. J., Waldman, R., Livne, E., & Blondin, S. 2012, *MNRAS*, 426, L76
 Dessart, L., Waldman, R., Livne, E., Hillier, D. J., & Blondin, S. 2013, *MNRAS*, 428, 3227
 Drout, M. R., Soderberg, A. M., Gal-Yam, A., et al. 2011, *ApJ*, 741, 97
 Ekström, S., Georgy, C., Eggenberger, P., et al. 2012, *A&A*, 537, A146
 Fabricant, D., Cheimets, P., Caldwell, N., & Geary, J. 1998, *PASP*, 110, 79
 Gal-Yam, A. 2012, *Science*, 337, 927
 Gal-Yam, A., Mazzali, P., Ofek, E. O., et al. 2009, *Nature*, 462, 624
 Galama, T. J., Vreeswijk, P. M., van Paradijs, J., et al. 1998, *Nature*, 395, 670
 Hjorth, J., & Bloom, J. S. 2012, *The Gamma-Ray Burst - Supernova Connection*, 169
 Howerton, S., Drake, A. J., Djorgovski, S. G., et al. 2012, *Central Bureau Electronic Telegrams*, 3052, 1
 Hsiao, E. Y., Marion, G. H., Phillips, M. M., et al. 2013, *ArXiv e-prints*, arXiv:1301.6287 [astro-ph.CO]
 Iwamoto, K., Mazzali, P. A., Nomoto, K., et al. 1998, *Nature*, 395, 672
 Iwamoto, K., Nakamura, T., Nomoto, K., et al. 2000, *ApJ*, 534, 660
 Jeffery, D. J., Ketchum, W., Branch, D., et al. 2007, *ApJS*, 171, 493
 Kasen, D., & Bildsten, L. 2010, *ApJ*, 717, 245
 Langer, N., Norman, C. A., de Koter, A., et al. 2007, *A&A*, 475, L19
 Maeda, K., Mazzali, P. A., Deng, J., et al. 2003, *ApJ*, 593, 931
 Maeda, K., Mazzali, P. A., & Nomoto, K. 2006, *ApJ*, 645, 1331
 Maeda, K., & Nomoto, K. 2003, *ApJ*, 598, 1163
 Matheson, T., Filippenko, A. V., Li, W., Leonard, D. C., & Shields, J. C. 2001, *AJ*, 121, 1648
 Mazzali, P. A., Deng, J., Maeda, K., et al. 2004, *ApJ*, 614, 858
 Milisavljevic, D., Fesen, R. A., Gerardy, C. L., Kirshner, R. P., & Challis, P. 2010, *ApJ*, 709, 1343
 Minkowski, R. 1941, *PASP*, 53, 224
 Moriya, T., Tominaga, N., Tanaka, M., Maeda, K., & Nomoto, K. 2010, *ApJ*, 717, L83
 Nomoto, K., Maeda, K., Nakamura, T., et al. 2000, in *American Institute of Physics Conference Series*, Vol. 526, *Gamma-ray Bursts*, 5th Huntsville Symposium, ed. R. M. Kippen, R. S. Malozzi, & G. J. Fishman, 622
 Patat, F., Cappellaro, E., Danziger, J., et al. 2001, *ApJ*, 555, 900
 Pettini, M., & Pagel, B. E. J. 2004, *MNRAS*, 348, L59
 Poznanski, D., Prochaska, J. X., & Bloom, J. S. 2012, *MNRAS*, 426, 1465
 Quimby, R. M., Kulkarni, S. R., Kasliwal, M. M., et al. 2011, *Nature*, 474, 487
 Sanders, N. E., Soderberg, A. M., Levesque, E. M., et al. 2012, *ApJ*, 758, 132
 Schlafly, E. F., & Finkbeiner, D. P. 2011, *ApJ*, 737, 103
 Schmidt, G. D., Weymann, R. J., & Foltz, C. B. 1989, *PASP*, 101, 713
 Silverman, J. M., Cenko, S. B., Miller, A. A., Nugent, P. E., & Filippenko, A. V. 2012, *Central Bureau Electronic Telegrams*, 3052, 2
 Simcoe, R. A., Burgasser, A. J., Bernstein, R. A., et al. 2008, in *Society of Photo-Optical Instrumentation Engineers (SPIE) Conference Series*, Vol. 7014, *Society of Photo-Optical Instrumentation Engineers (SPIE) Conference Series*
 Soderberg, A. M., Berger, E., Page, K. L., et al. 2008, *Nature*, 453, 469

- Soderberg, A., Dittmann, J., Claus, B., et al. 2012, The Astronomer's Telegram, 3968, 1
- Tanaka, M., Yamanaka, M., Maeda, K., et al. 2009, ApJ, 700, 1680
- Taubenberger, S., Valenti, S., Benetti, S., et al. 2009, MNRAS, 397, 677
- Theureau, G., Hanski, M. O., Coudreau, N., Hallet, N., & Martin, J.-M. 2007, A&A, 465, 71
- Thomas, R. C., Nugent, P. E., & Meza, J. C. 2011, PASP, 123, 237
- Valenti, S., Benetti, S., Cappellaro, E., et al. 2008, MNRAS, 383, 1485
- Van Dyk, S. D., Cenko, S. B., Silverman, J. M., et al. 2012, The Astronomer's Telegram, 3971, 1
- Yoshida, T., & Umeda, H. 2011, MNRAS, 412, L78
- Young, D. R., Smartt, S. J., Valenti, S., et al. 2010, A&A, 512, A70

Table 1
UV/Optical Photometry

MJD	<i>uvm2</i>	<i>uvw2</i>	<i>uvw1</i>	<i>u</i>	<i>b</i>	<i>v</i>	SDSS <i>r'</i>	Telescope/Instr.
56001.74	15.91 0.06	15.74 0.07	14.72 0.06	13.52 0.05	14.11 0.04	13.67 0.04	...	<i>Swift</i> -UVOT
56004.75	16.00 0.07	15.87 0.07	14.87 0.06	13.59 0.05	14.03 0.04	13.56 0.04	...	<i>Swift</i> -UVOT
56005.95	15.95 0.09	15.91 0.08	15.02 0.07	13.65 0.05	14.02 0.05	13.51 0.05	...	<i>Swift</i> -UVOT
56006.80	16.09 0.07	15.95 0.07	15.02 0.06	13.78 0.05	14.05 0.04	13.54 0.04	...	<i>Swift</i> -UVOT
56007.79	16.06 0.07	15.99 0.07	15.13 0.06	13.88 0.05	14.09 0.04	13.51 0.04	...	<i>Swift</i> -UVOT
56011.76	16.32 0.07	16.24 0.08	15.59 0.06	14.39 0.05	14.38 0.05	13.61 0.04	...	<i>Swift</i> -UVOT
56020.18	16.57 0.07	16.55 0.08	16.14 0.06	15.46 0.06	15.16 0.05	14.15 0.04	...	<i>Swift</i> -UVOT
56026.48	16.50 0.07	16.47 0.08	...	15.78 0.06	15.57 0.05	14.61 0.05	...	<i>Swift</i> -UVOT
56029.61	16.57 0.07	16.56 0.08	16.45 0.07	15.81 0.06	15.66 0.05	14.63 0.04	...	<i>Swift</i> -UVOT
56033.62	16.59 0.07	16.62 0.08	16.42 0.07	15.95 0.06	15.76 0.05	14.73 0.04	...	<i>Swift</i> -UVOT
56035.60	16.55 0.07	16.45 0.08	16.32 0.07	15.95 0.06	15.85 0.05	14.84 0.05	...	<i>Swift</i> -UVOT
56038.46	16.64 0.07	16.56 0.08	16.41 0.07	15.95 0.06	15.86 0.05	14.88 0.05	...	<i>Swift</i> -UVOT
56315.43	16.95 0.10	MDM/OSMOS
56341.52	17.94 0.13	MMT/MMTcam

Note. — Uncertainties are adjacent to measurements and are at the 68% confidence level.